

## ATMOSPHERIC SCIENCE

## Shipborne eddy covariance observations of methane fluxes constrain Arctic sea emissions

Brett F. Thornton<sup>1,2\*</sup>, John Prytherch<sup>2,3</sup>, Kristian Andersson<sup>1</sup>, Ian M. Brooks<sup>4</sup>, Dominic Salisbury<sup>4</sup>, Michael Tjernström<sup>2,3</sup>, Patrick M. Crill<sup>1,2</sup>

We demonstrate direct eddy covariance (EC) observations of methane (CH<sub>4</sub>) fluxes between the sea and atmosphere from an icebreaker in the eastern Arctic Ocean. EC-derived CH<sub>4</sub> emissions averaged 4.58, 1.74, and 0.14 mg m<sup>-2</sup> day<sup>-1</sup> in the Laptev, East Siberian, and Chukchi seas, respectively, corresponding to annual sea-wide fluxes of 0.83, 0.62, and 0.03 Tg year<sup>-1</sup>. These EC results answer concerns that previous diffusive emission estimates, which excluded bubbling, may underestimate total emissions. We assert that bubbling dominates sea-air CH<sub>4</sub> fluxes in only small constrained areas: A ~100-m<sup>2</sup> area of the East Siberian Sea showed sea-air CH<sub>4</sub> fluxes exceeding 600 mg m<sup>-2</sup> day<sup>-1</sup>; in a similarly sized area of the Laptev Sea, peak CH<sub>4</sub> fluxes were ~170 mg m<sup>-2</sup> day<sup>-1</sup>. Calculating additional emissions below the noise level of our EC system suggests total ESAS CH<sub>4</sub> emissions of 3.02 Tg year<sup>-1</sup>, closely matching an earlier diffusive emission estimate of 2.9 Tg year<sup>-1</sup>.

## INTRODUCTION

The emission of methane (CH<sub>4</sub>) to the atmosphere in the Arctic has become a major research focus in the past decade, alongside suggestions that these emissions may increase as a response to global warming, leading to a self-reinforcing warming effect (1). In particular, there remains substantial uncertainty in the scale of sea to atmosphere emissions of CH<sub>4</sub> in the Arctic (2–6). Of notable interest are the expansive (2.1 million km<sup>2</sup>) and relatively shallow East Siberian Arctic Shelf (ESAS) seas off the Russian and Alaskan Arctic coasts [the Laptev, East Siberian, and Chukchi seas, with mean depths of 48, 58, and 80 m, respectively (7)], which are partly underlain by relic permafrost formed during the low sea level at the Last Glacial Maximum, when much of these seas' present area was land above sea level (asl). The permafrost sediments could be a source of CH<sub>4</sub> as they slowly thaw, or CH<sub>4</sub> could exist as deeper clathrate sources, perhaps exposed on the continental slopes (8).

However, CH<sub>4</sub> released at the seafloor or in thawing subsea permafrost does not necessarily reach the atmosphere (9). In particular, it may dissolve in and be oxidized in the water column (5, 9–11), become trapped below the pycnocline (12), and be lost in the sulfate reduction zone just below the sediment-seawater interface (13) or even deep in the sediment itself (14). For this reason, reliable methods of determining the sea to atmosphere emissions are needed, especially in regions with highly spatially heterogeneous fluxes, such as above seafloor gas seeps.

Estimates of the sea-to-atmosphere emissions from the ESAS have ranged up to 17 Tg year<sup>-1</sup> (2), ~28% of the total bottom-up (adding up sources) Arctic CH<sub>4</sub> emission, and ~75% of the top-down inverse modeled Arctic CH<sub>4</sub> emissions (15, 16). These large marine emissions would leave inadequate room for other better-understood terrestrial Arctic sources of CH<sub>4</sub> in the budget and/or the entire Arctic CH<sub>4</sub> budget is underestimated [e.g., (15)].

<sup>1</sup>Department of Geological Sciences, Stockholm University, 106 91 Stockholm, Sweden. <sup>2</sup>Bolin Centre for Climate Research, Stockholm University, 106 91 Stockholm, Sweden. <sup>3</sup>Department of Meteorology, Stockholm University, 106 91 Stockholm, Sweden. <sup>4</sup>School of Earth and Environment, University of Leeds, Leeds, UK.

\*Corresponding author. Email: brett.thornton@geo.su.se

Here, we use direct eddy covariance (EC) measurements of CH<sub>4</sub> fluxes in the Laptev, East Siberian, and Chukchi seas during the 2014 SWERUS-C3 expedition to better understand the ultimate sea-atmosphere flux of CH<sub>4</sub> under various summertime Arctic sea conditions including open water and partial and complete sea ice cover and above seafloor gas seeps. We build on an earlier analysis of SWERUS-C3 diffusive CH<sub>4</sub> fluxes calculated from atmospheric and surface water CH<sub>4</sub> concentration measurements in the Laptev and East Siberian seas using a bulk flux model. We demonstrate that EC measurements of the sea-air CH<sub>4</sub> flux can be a powerful tool in locating and quantifying sea-air emission hot spots, without the use of any waterside measurements of CH<sub>4</sub>.

## RESULTS

CH<sub>4</sub> emissions to the atmosphere were apparent throughout the study area (Table 1), presumably because of widespread supersaturation of CH<sub>4</sub> in the surface waters (4). The Arctic Ocean proper was sampled during two cruise segments: first, between the northern Kara Sea and the Laptev Sea [day of year (DoY) 192 to 198]; second, an additional transect out of the Laptev Sea into the Arctic Ocean during DoY 205 to 207 (Fig. 1). The region sampled is adjacent to the Laptev and Kara seas, and these data should not be interpreted as representative of the entire Arctic Ocean proper. Overall, the EC CH<sub>4</sub> flux here was 0.12 mg m<sup>-2</sup> day<sup>-1</sup>. The first Arctic Ocean region sampled, north of the Laptev Sea, was ice covered, while the second region was ice free; we determined near-zero EC CH<sub>4</sub> fluxes of 0.13 and 0.09 mg m<sup>-2</sup> day<sup>-1</sup> in the two regions, respectively.

We treated the shelf breaks and upper continental slopes of the ESAS as a separate region due to speculation that decomposing CH<sub>4</sub> hydrates on continental slopes [e.g., (17, 18)] may be providing an additional CH<sub>4</sub> source to the atmosphere in these regions. Although *Oden* was in this region for long time periods during SWERUS-C3, accounting for about 10% of the flux measurements, the EC flux was indistinguishable from zero (0.09 mg m<sup>-2</sup> day<sup>-1</sup>; Table 1), although previously reported diffusive flux estimates for this region were slightly higher at 1.4 mg m<sup>-2</sup> day<sup>-1</sup> (4), a small positive flux due to CH<sub>4</sub> supersaturation in surface water.

Copyright © 2020  
The Authors, some  
rights reserved;  
exclusive licensee  
American Association  
for the Advancement  
of Science. No claim to  
original U.S. Government  
Works. Distributed  
under a Creative  
Commons Attribution  
NonCommercial  
License 4.0 (CC BY-NC).

**Table 1. EC average sea-air CH<sub>4</sub> fluxes by region (in ng m<sup>-2</sup> s<sup>-1</sup> and mg m<sup>-2</sup> day<sup>-1</sup>).** Regions marked with \* are the same regions as used in table 2 of (4) for calculated sea-air CH<sub>4</sub> fluxes. Note that many of the regions are overlapping. "Seeps only" is defined as stations/areas with EC CH<sub>4</sub> measurements >6 mg m<sup>-2</sup> day<sup>-1</sup> (see Table 2 for locations).

	Spatially normalized fluxes			No. of EC measurement locations
	Average (ng m <sup>-2</sup> s <sup>-1</sup> )	Average (mg m <sup>-2</sup> day <sup>-1</sup> )	Maximum (mg m <sup>-2</sup> day <sup>-1</sup> )	
Arctic Ocean*	1.39	0.12	6.3	349
Shelf breaks and upper continental slope*	1.01	0.09	6.4	241
Shelf seas (Laptev + East Siberian + Chukchi seas)	17.3	1.50	618	1851
Laptev Sea (all)*	53.1	4.58	170	265
Laptev Sea, seeps only	363	21.4	170	32
East Siberian Sea (all)	20.2	1.74	618	834
East Siberian Sea, ice-covered/melt regions (<DoY 222.3)*	23.5	2.02	618	695
East Siberian Sea, ice-covered/melt regions	24.1	2.09	618	677
East Siberian Sea, ice-free	3.17	0.27	8.6	157
East Siberian Sea, seeps only	1004	63.3	618	17
Chukchi Sea, ice-free	2.51	0.22	8.4	429
Chukchi Sea, ice-covered/melt regions	0.39	0.03	8.3	326
Chukchi Sea (all)	1.62	0.14	8.4	755

The studied portion of the Laptev Sea was ice free during SWERUS-C3. The average flux from the two seep regions in the Laptev was 21.4 mg m<sup>-2</sup> day<sup>-1</sup>, somewhat similar to typical terrestrial subarctic wetland emission rates (19). The enhanced emissions extended over a total of 6.4 km<sup>2</sup> of the Laptev Sea, on the continental shelf, in waters 65 m deep (Table 2). Fluxes from the entire Laptev averaged 4.58 mg m<sup>-2</sup> day<sup>-1</sup>, more than an order of magnitude higher than fluxes seen from the adjacent Arctic Ocean regions and above the shelf break and continental slope.

The ice-free portion of the East Siberian Sea we sampled exhibited lower EC CH<sub>4</sub> fluxes than the ice-free portions of the Laptev Sea, only 0.27 mg m<sup>-2</sup> day<sup>-1</sup> (Table 1). In contrast, the ice-covered (including partial ice cover) portion of the East Siberian showed a higher average flux (2.09 mg m<sup>-2</sup> day<sup>-1</sup>) and was characterized as undergoing rapid ice melt during SWERUS-C3, with much slushy ice and openings in the ice (4, 20). In this ice-covered portion, seven seeps were encountered on the basis of EC measurements (Table 2), with a total areal extent estimated at 47.2 km<sup>2</sup> and an average flux of 63.3 mg m<sup>-2</sup> day<sup>-1</sup>. Although sonar revealed seafloor gas seeps at these locations, it can be difficult to positively separate the source of these high fluxes into bubbles directly reaching the surface and bubbles trapped in ice being released by ship movement through the ice or ice melt, which may have contributed to some of the higher fluxes seen at these East Siberian Sea areas compared with those in the Laptev Sea. Overall, a larger area of enhanced surface seawater CH<sub>4</sub> concentrations was observed in the East Siberian Sea compared to the Laptev Sea during SWERUS-C3 (4).

No seafloor gas seeps were encountered in the Chukchi Sea except for a scattered few in the Herald Canyon area, as was noted previ-

ously (21). Localized EC CH<sub>4</sub> sea-air fluxes near these gas seeps, and elsewhere in the Chukchi Sea, were not large enough to significantly increase Chukchi Sea total CH<sub>4</sub> emissions. CH<sub>4</sub> emissions were slightly larger in open water than in ice-covered and partially ice-covered regions of the Chukchi Sea, but the overall flux from the Chukchi Sea of 0.14 mg m<sup>-2</sup> day<sup>-1</sup> was below any of the other shelf sea regions.

Although the area of enhanced emissions around the visited seafloor seeps was substantially larger in the East Siberian than in the Laptev Sea, the sea ice coverage in the East Siberian Sea complicates interpretation of these results. Substantial CH<sub>4</sub> may have been trapped beneath or within the ice and potentially released by the movement of the icebreaker through the area. However, because the EC footprint is upwind of the bow for all measurements within the accepted wind sector, only in slow back and forth or circling maneuvering (which would be limited to a small number of spatially normalized measurements) could this CH<sub>4</sub> source be a significant contribution to our measured fluxes; we do not believe that these emissions occurred to any significant extent during the cruise.

The East Siberian Sea is presently ice covered about 70% of each year, limiting sea-air gas exchange. However, CH<sub>4</sub> could escape through polynyas or be trapped in the ice and be released later, so we can calculate a maximum annual flux for these two seep areas: For the 6.4 km<sup>2</sup> of observed Laptev Sea seeps, the annual sea-air CH<sub>4</sub> flux would be 50,000 kg year<sup>-1</sup>. In the 47.3-km<sup>2</sup> seep area in the East Siberian Sea, the annual sea-air CH<sub>4</sub> flux would be 1.094 × 10<sup>6</sup> kg year<sup>-1</sup>.

Our Chukchi Sea fluxes are broadly consistent with an earlier study in the area (21), which reported fluxes of 0.087 to 0.91 mg m<sup>-2</sup> day<sup>-1</sup>, based on waterside dissolved CH<sub>4</sub> measurements. Two other studies noted CH<sub>4</sub> supersaturation in the Chukchi Sea: (8.05 ± 0.05 nM)

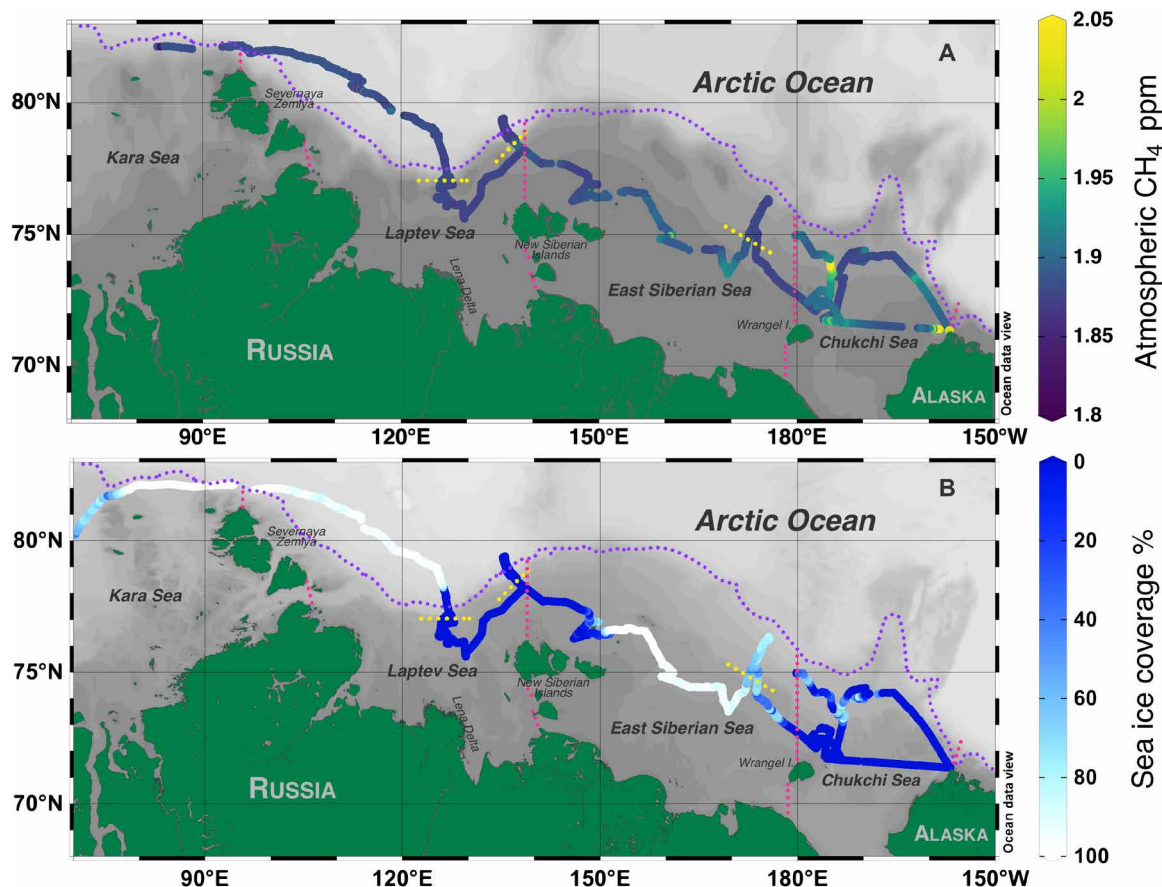


**Fig. 1. SWERUS-C3 cruise in the Arctic Ocean during July to August 2014.** The dotted purple lines indicate the approximate extent of shelf seas after (7). Dotted magenta lines divide shelf seas. Dotted yellow lines indicate the approximate location of the top of the continental slope in Laptev and East Siberian seas. (A) Atmospheric CH<sub>4</sub> concentrations (ppm) during SWERUS-C3 (until DoY 240). This figure includes data from figure 1a from (4), extended with additional measurements after DoY 222 in the Chukchi and East Siberian seas. (B) Sea ice coverage (%) at *Oden's* position during SWERUS-C3 from AMSR2 satellite retrievals.

in the Bering and western Chukchi seas combined (22); similar values were reported for the eastern Chukchi of 3.0 to 7.3 nM (23). Reports to date, including this study, suggest that the Chukchi Sea, despite being geologically connected to the ESAS, is a smaller contributor to atmospheric CH<sub>4</sub> than either the East Siberian Sea or Laptev Sea.

Pan-ESAS CH<sub>4</sub> emissions determined from our EC system during SWERUS-C3 are estimated at 1.49 Tg CH<sub>4</sub> year<sup>-1</sup> (Table 3). It is important to point out that earlier studies have often extrapolated across the ESAS area, including the Chukchi Sea, while having few or no actual measurements within Chukchi. Our data and (21–23) suggest that Chukchi Sea CH<sub>4</sub> emissions are markedly smaller than emissions from the Laptev and East Siberian seas, making extrapolated ESAS emission estimates, which assume similar emission distributions across all three seas likely overestimations.

As discussed in Materials and Methods, the 2σ noise of a single 20-min EC CH<sub>4</sub> flux measurement if the actual flux was ~0 mg m<sup>-2</sup> day<sup>-1</sup> is 2 mg m<sup>-2</sup> day<sup>-1</sup>. This is close to the average calculated diffusive flux (2.99 mg m<sup>-2</sup> day<sup>-1</sup>) for the entire ESAS (4) and with many EC CH<sub>4</sub> single observations being close to or within the noise (although noise is reduced by averaging multiple observations, as each EC measurement is independent). How much CH<sub>4</sub> emission, averaged over the entire ESAS, could be present in the noise of the EC measurement? Assuming a small ESAS-wide sea-to-atmosphere flux of 2 mg m<sup>-2</sup> day<sup>-1</sup>, the total “missed” flux would only be 1.53 Tg CH<sub>4</sub> year<sup>-1</sup>. Adding this

potentially “missed” flux to the net EC flux of 1.49 Tg CH<sub>4</sub> year<sup>-1</sup> yields a sum of 3.02 Tg CH<sub>4</sub> year<sup>-1</sup>, a value notably close to the 2.9 Tg year<sup>-1</sup> we determined by diffusive flux emissions alone (4).

## DISCUSSION

### Peak CH<sub>4</sub> sea-to-atmosphere fluxes

The seep areas encountered during SWERUS-C3 showed impressively large peak fluxes, but these seeps alone are a negligible contribution to regional sea-air fluxes (Table 3). The largest emissions we observed are likely a combination of CH<sub>4</sub> resupply to the surface waters by bubbles plus direct bubble transport to the atmosphere. Assuming that the spatial seep occurrence density of 2.01% (defined as percentage of all EC measurements >6 mg m<sup>-2</sup> d<sup>-1</sup>) observed during SWERUS-C3 is similar for the entire ESAS suggests that fluxes directly above seeps contribute only ~1144 metric tons of CH<sub>4</sub> per year to the atmosphere. This is only 0.039% of the ESAS annual diffusive flux (2.9 Tg year<sup>-1</sup>) reported earlier (4). Thus, as suggested in (4), it seems likely that seeps depositing CH<sub>4</sub> in the upper layers of the sea, from where it later diffuses into atmosphere, represent a larger CH<sub>4</sub> emission source than direct bubble transport to the atmosphere. Many, many more seep areas similar to those we studied are required for the direct bubble-to-atmosphere injection of CH<sub>4</sub> to be a significant contributor to the sea-air flux from the ESAS.

**Table 2. Locations and peak and average CH<sub>4</sub> EC sea-air CH<sub>4</sub> fluxes from Laptev Sea and East Siberian Sea seep areas sampled during SWERUS-C3.** 2 $\sigma$  error is  $\pm 2 \text{ mg m}^{-2} \text{ day}^{-1}$  for peak (single measurement) flux observations. Areal extent of each seep area is determined by the distance from peak flux of first measurement  $< 6 \text{ mg m}^{-2} \text{ day}^{-1}$  CH<sub>4</sub>, a very conservative assumption that seep area extends this distance from peak. EC measurement locations refer to discrete measurement locations in the spatially normalized dataset, not the total number of EC measurements. All data are after filtering. LS1, LS2, ESS1, ESS2, and ESS7 are displayed in Fig. 2.

Peak latitude (°N)	Peak longitude (°E)	Peak CH <sub>4</sub> flux (mg m <sup>-2</sup> day <sup>-1</sup> )	Average CH <sub>4</sub> flux (mg m <sup>-2</sup> day <sup>-1</sup> )	Estimated areal extent of fluxes $> 6 \text{ mg m}^{-2} \text{ day}^{-1}$ (km <sup>2</sup> )	EC measurement locations within enhanced area
76.7742 (LS1)	125.8331	170	36.0	2.0	25
76.8884 (LS2)	127.7762	33.1	14.8	4.4	7
74.9571 (ESS1)	161.0839	618	142	9.4	4
74.9913 (ESS2)	161.1423	114	29.6	18.8	7
74.9099 (ESS3)	160.4246	54.2	43.4	6.3	2
74.4200 (ESS4)	166.9303	11.8	11.8	0.5	1
74.4376 (ESS5)	167.3439	17.6	17.6	5.4	1
73.8477 (ESS6)	170.3830	17.2	17.2	3.9	1
74.1982 (ESS7)	171.3923	221	221	3.0	1
Area weighted fluxes					
Laptev Sea seep areas			21.4	6.4	32
East Siberian Sea seep areas			63.3	47.3	17

### Quantifying fluxes above seafloor gas seeps

At least one previous study (24) has described the difference between measured EC flux and calculated bulk (diffusive) flux as the ebullition flux—the direct injection of CH<sub>4</sub> into the atmosphere from bubbles. Although superficially appealing, caution should be used when comparing direct and bulk estimates of surface fluxes. (More discussion of this concern is provided in Materials and Methods.) For example, in the immediate vicinity of the seep region in the Laptev Sea, a maximum calculated diffusive flux of  $83 \text{ mg m}^{-2} \text{ day}^{-1}$  was reported within 100 m of the peak flux and  $58 \text{ mg m}^{-2} \text{ day}^{-1}$  up to 1 km from the seep (4). The larger of the two Laptev Sea EC flux peaks (LS1; Table 2) seen in our EC data reached  $170 \text{ mg m}^{-2} \text{ day}^{-1}$ , over an area of  $\sim 2 \text{ km}^2$ . Although the peak EC estimate is about double the peak bulk estimate of the diffusive flux, it is not possible to ascribe half of the EC flux to a direct injection of CH<sub>4</sub> from bubbles without knowing far more about the spatial structure of both the sea-air concentration difference and EC flux than we actually do, requiring high-resolution gridded sampling (at about an order of magnitude below the EC footprint size) of surface water CH<sub>4</sub> concentrations across the seep field. It does, however, seem nearly certain that some fraction of the EC flux observed at seep sites does come from direct bubble injection of CH<sub>4</sub> into the atmosphere.

### Chukchi Sea enhancements in atmospheric CH<sub>4</sub>

In the Chukchi Sea, despite the notable lack of sea-air EC CH<sub>4</sub> flux enhancements (Fig. 2), the highest atmospheric CH<sub>4</sub> concentrations of the entire cruise were observed (Fig. 1A), near the Alaskan coast north of Barrow. However, the lack of any corresponding sea-air fluxes in the Chukchi Sea sufficient to create these atmospheric concentrations leads us to suspect that these enhancements over the  $\sim 1.875$ -ppm (parts per million) background were not local in origin but transported from other areas. We used the online National Oceanic and Atmospheric Administration (NOAA) Hybrid Single-Particle

Lagrangian Integrated Trajectory (HYSPPLIT) model (25) to compute back trajectories for certain areas with enhanced atmospheric CH<sub>4</sub>. Four-day HYSPPLIT back trajectories (figs. S2 and S3) from the peak in observed CH<sub>4</sub> atmospheric concentrations (2.06 ppm) on DoY 239 at approximately 73.92°N, 175.91°W suggest that this air had spent much of the past 4 days in the ESAS region, including over coastal zones. The near-Alaskan shore atmospheric CH<sub>4</sub> enhancements (reaching  $\sim 2.1$  ppm) on DoY 233 at approximately 71.41°N, 158.96°W show a clear non-Arctic Ocean back trajectory. Seafloor gas seeps have been reported in the Chukchi Sea, notably in the Herald Canyon area (21), but we observed no large flux increases in this area.

### Emissions from shallower regions of the ESAS

The studied depths in (2) are far shallower (6-m minimum depth and 24-m maximum depth) areas of the Laptev Sea near the Lena Delta, in comparison to our present study and (4) (minimum depth, 35 m). As bubbles are expected to be significantly stripped of CH<sub>4</sub> as they transit the water column (9), it is reasonable to expect that the seafloor seeps encountered in (2) would transport more CH<sub>4</sub> to the atmosphere than those encountered in (4) and the present study; thus, it is reasonable to expect that bubbles represent a larger percentage of the total CH<sub>4</sub> flux to the atmosphere in shallow regions of the ESAS. This is especially important when extrapolating fluxes to the entire shelf area. It is unclear to us whether this was taken into account when determining an entire ESAS bubble flux ( $9 \text{ Tg year}^{-1}$ ) from sonar bubble counting; rather, it appears that the fluxes were determined by bubbling rates at the seafloor seeps without accounting for water column loss processes (2). [We acknowledge that the argument implied in (2) is that dissolved CH<sub>4</sub> could be readily ventilated by storm events before oxidation in the water column.]

Following the assumption of (2) that bubble size is not correlated with seep rate, we note that a 7.5-mm-diameter bubble, the size

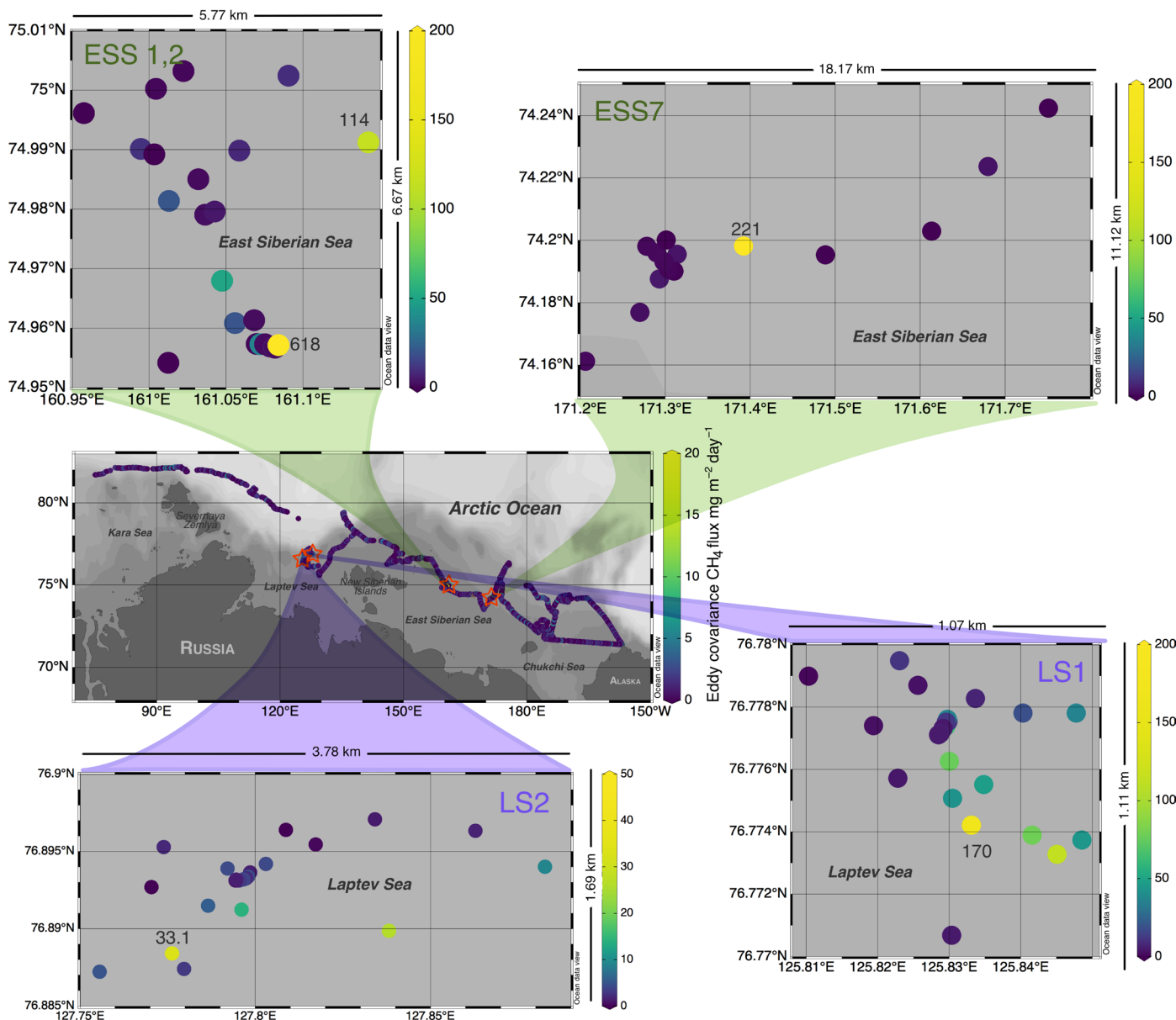


**Fig. 2. Measured sea-air EC CH<sub>4</sub> flux (mg m<sup>-2</sup> day<sup>-1</sup>) during SWERUS-C3 until DoY 240 with insets for selected seep regions.** Red open stars on the main map show the approximate location of each seep area. The spatial extent of each inset map is shown above and to the right of each inset. Note that the color scale varies between the main plot and insets.

estimated in table 1 of (2), would only transmit ~65% of its initial CH<sub>4</sub> to the surface in 15 m of water. At the average depth of the Laptev and East Siberian seas, only ~20% of the initial CH<sub>4</sub> would be expected to reach the ocean surface and enter the atmosphere (9). We can use these models, observations, and data from (2) to estimate the CH<sub>4</sub> flux from shallowest areas of the ESAS not studied in SWERUS-C3 or other studies.

First, in shallowest areas of the ESAS, <5 m, nearly 100% of the CH<sub>4</sub> released at the sediment is expected to reach the atmosphere. However, waters of these shallowest depths account for only ~3.3% of the ESAS shelf seas' total area (7). These shallowest ESAS regions could add ~0.18 Tg CH<sub>4</sub> year<sup>-1</sup> of ebullitive flux to the total ESAS CH<sub>4</sub> emissions and 0.15 Tg CH<sub>4</sub> year<sup>-1</sup> via diffusive emissions as-

suming bubble emissions as described in (2) and diffusive emissions as described in (24). Thus, we estimate total <5-m flux across the ESAS to be 0.33 Tg CH<sub>4</sub> year<sup>-1</sup>.

Second, the depth range of 5 to 35 m accounts for 39.3% of the ESAS area, and the surveys reported in (2, 24) sampled this range extensively. Accounting for the variable bubble transmission efficiency over this depth range (9), we estimate the bubble CH<sub>4</sub> flux from 5- to 35-m depth range to be 0.10, 0.48, and 0.32 Tg year<sup>-1</sup> for the Chukchi, East Siberian, and Laptev seas, respectively. We also took the 4.47 Tg CH<sub>4</sub> year<sup>-1</sup> for diffusive flux across the entire ESAS from (24) and extracted emissions for the 5- to 35-m depth range only. This is an additional 1.76 Tg CH<sub>4</sub> year<sup>-1</sup>, giving a net 5- to 35-m flux of 2.66 Tg year<sup>-1</sup> across the ESAS.

**Table 3. ESAS CH<sub>4</sub> sea-air flux results and comparisons with earlier studies.** Annual EC fluxes assume that 100% of CH<sub>4</sub> trapped in or under ice for part of the year eventually reaches the atmosphere. The whole-ESAS CH<sub>4</sub> emission estimate from EC fluxes is lower than estimates given in three earlier measurement-based studies (2, 4, 24), shown at the bottom of this table. Part of this difference is due to the inclusion of the Chukchi Sea in the present study, which accounts for 29.4% of the ESAS area and had markedly lower sea-air fluxes than the Laptev or East Siberian seas, the two seas that the earlier three studies based their results solely on. Inclusion of low flux observations from the Chukchi Sea in the earlier measurement-based studies could have reduced pan-ESAS areal flux estimates in all of them. The flux values in (24) were reported in Tg C-CH<sub>4</sub> year<sup>-1</sup> and have been converted to Tg CH<sub>4</sub> year<sup>-1</sup> here in Table 3. Extrapolating the whole-ESAS fluxes from only our observed Laptev Sea and East Siberian Sea regional fluxes, as in previous studies (2, 4, 24), we obtain the slightly higher annual CH<sub>4</sub> flux estimate of 2.43 mg m<sup>-2</sup> day<sup>-1</sup> or 2.07 Tg year<sup>-1</sup>. This is still the lowest whole-ESAS value yet reported based on in situ measurements but is closest to the recent bulk flux measurement from the same cruise (Table 3) and is within the range of the only inverse modeling study for the ESAS region (3). The highest value, 4.65 Tg year<sup>-1</sup>, is obtained by combining the data of (2, 24) for depths <35 m with (4) for deeper waters and accounting for bubble losses using the model of (9). Estimating small fluxes possibly missed by the EC system due to the EC noise levels, we add 1.53 Tg year<sup>-1</sup> to our total (see text for explanation). This is our best estimate for pan-ESAS CH<sub>4</sub> fluxes based on SWERUS-C3 data alone and is close to the 2.9 Tg year<sup>-1</sup> of (4).

Shelf Sea*	Sea area (×10 <sup>3</sup> km <sup>2</sup> )	Calculated bulk flux <sup>†</sup> (mg m <sup>-2</sup> day <sup>-1</sup> )	(EC) CH <sub>4</sub> flux (mg m <sup>-2</sup> day <sup>-1</sup> )	Annual (EC) CH <sub>4</sub> flux (Tg year <sup>-1</sup> )
Laptev	498	3.90	4.58	0.83
East Siberian	987	3.7 (13.8) <sup>‡</sup>	1.74	0.62
Chukchi	620	No data	0.14	0.03
ESAS	2105	–	1.94	1.49
ESAS (extrapolation without Chukchi data as in previous studies)	1485	3.8 (12.3) <sup>‡</sup>	2.43	2.07
ESAS [EC + estimated flux in EC noise (present study)]	2105	–	–	3.02
ESAS [0- to 35-m depth range based on (24) and (2) + depth-based bubble dissolution model; >35-m depths based on (4)].	2105	–	–	4.65
Previous studies (method used)				
			Areal flux	Annual flux
ESAS (3) (inverse model)			0–5.9	0–4.5
ESAS (2) (ebullition only; bubble counting with sonar)			22.1	9 <sup>§</sup>
ESAS (24) (various measurements, primarily surface water concentrations)			13.9	10.6
ESAS (4) (surface water and atmospheric concentrations; Laptev and East Siberian seas only)			3.8	2.9

\*Sea areas defined as in (7). †Calculated bulk fluxes are from data presented in (4). ‡Calculated bulk flux values in parentheses include ice-covered areas, where calculated fluxes are hypothetical, and may represent temporary ice-out fluxes. §Total ESAS annual CH<sub>4</sub> flux including diffusive emissions was reported as 17 Tg year<sup>-1</sup> in (2).

Last, we assume that the present study and (4) adequately sample ESAS waters deeper than 35 m (57.3% of the ESAS area), so we use the diffusive flux estimates presented earlier (4) for this depth range. Again, we scale these diffusive flux values down to reflect the relative contributions of each sea. Thus, the pan-ESAS flux would be 1.66 CH<sub>4</sub> Tg year<sup>-1</sup> for waters with a depth of >35 m based on (4). Both the present EC study and (4) show that this mid and outer shelf region's CH<sub>4</sub> emissions are dominated by diffusive emissions, although there is certainly a small direct bubble flux contribution.

We recognize that many assumptions have been made in the analysis we have described in this section using data from earlier studies with vastly different methodologies. However, summing these three depth regions (<5, 5 to 35, and >35 m), we obtain 4.65 Tg CH<sub>4</sub> year<sup>-1</sup> for ebullitive and diffusive fluxes combined. This is larger than the 3.02 Tg CH<sub>4</sub> year<sup>-1</sup> of the present study or the 2.9 Tg year<sup>-1</sup> of (4).

A whole-ESAS flux of 4.65 Tg CH<sub>4</sub> year<sup>-1</sup> is on the high end of a regional inversion model estimate (3). Because this value (4.65 Tg CH<sub>4</sub> year<sup>-1</sup>) comes from multiple studies and relies on multiple types of measurements and extrapolations, we cannot assign great certainty to it. However, we do not doubt that there are additional bubble emissions in shallower waters than were surveyed during SWERUS, and this analysis suggests that total shallow emissions sum to something less than 2 Tg year<sup>-1</sup>.

## OUTLOOK AND CONCLUSION

This present study offers only a snapshot of the sea-air CH<sub>4</sub> flux situation in the ESAS during the late summer 2014. The 2014 data cannot exclude scenarios such as seep CH<sub>4</sub> outputs changing over time, resulting in higher or lower local sea-air fluxes. It is important

to consider that decreases in annual Arctic sea ice–covered days (26) may alter the sea-air CH<sub>4</sub> flux from the ESAS in the future, if CH<sub>4</sub> loss under or within sea ice is a significant process.

Peak emission rates from direct bubble CH<sub>4</sub> injection into the atmosphere will likely be missed if estimates are made using only calculated diffusive fluxes and/or surface water measurements. Detecting peak emissions requires, at present, sonar or EC methods. The peak sea-air flux we measured (618 mg m<sup>-2</sup> day<sup>-1</sup>) nearly matches a previously reported maximum sediment–water flux of 632 mg m<sup>-2</sup> day<sup>-1</sup> (estimated using sonar) (2). However, the spatial extent of the largest CH<sub>4</sub> fluxes to the atmosphere that we observed was about three orders of magnitude lower than the extent described for seep areas in that earlier work (2). Resolving this spatial extent discrepancy is an important future task. High bubble fluxes a few kilometers from the shore in the ESAS should not be extrapolated to the vast deeper regions farther offshore without a better understanding of the distribution of these high-flux regions. Accounting for small fluxes within the noise of our EC system, we estimate total ESAS CH<sub>4</sub> emissions at 3.02 Tg year<sup>-1</sup>. If emissions from shallower waters follow distributions suggested by (2, 24) for ESAS fluxes in <35-m-deep areas, this suggests a pan-ESAS annual flux of ~4.65 Tg CH<sub>4</sub> year<sup>-1</sup>.

We note an earlier report (6) of substantial CH<sub>4</sub> emissions from leads in the ice-covered Arctic Ocean far removed from the ESAS, so pan-Arctic Ocean total CH<sub>4</sub> emissions are almost certainly larger than our ESAS estimates. However, the lack of any strong regional atmospheric change in CH<sub>4</sub> in a model (3) supports our view of seafloor gas seeps depositing substantial CH<sub>4</sub> directly into the atmosphere as a mainly localized phenomena; however, bubbles transporting CH<sub>4</sub> above the pycnocline are likely significant for reloading surface waters with dissolved CH<sub>4</sub>. The EC methods described here should find use in mapping and searching for these high CH<sub>4</sub> emissions in other seas. We suggest that distributions of bubbles transporting significant amounts of CH<sub>4</sub> directly in the atmosphere via bubbling can be characterized using shipborne EC measurements.

## MATERIALS AND METHODS

Shipboard EC measurements of gas fluxes have been possible for some years (27); the general methodology is now established. However, shipboard EC measurements of CH<sub>4</sub> fluxes remain exceptionally rare with only indirectly reported results (24) and few detailed explanations of methods. A likely explanation for this rarity is that over most seas, the sea-air CH<sub>4</sub> fluxes are expected to be small and near the detection limit for EC systems, which only recently became suitable for these small CH<sub>4</sub> fluxes. It was recently postulated that higher sea-air CH<sub>4</sub> fluxes in the Arctic may make EC studies in this area viable (28).

The Swedish icebreaker *Oden* sailed from Tromsø, Norway on 5 July 2014 (DoY 186), reached Barrow, Alaska on 19 August 2014 (DoY 231), and then returned to Tromsø through the ESAS in August and September 2014 for the SWERUS-C3 cruise. During SWERUS-C3, we measured CH<sub>4</sub>, CO<sub>2</sub>, and H<sub>2</sub>O in the atmosphere at 10 Hz using a Los Gatos Research (LGR) cavity ring-down laser spectrometer (model 0010, FGGA 24EP, LGR, USA) (29). The system sampled air from a single inlet at the top of the meteorological mast at the bow of *Oden*, 20 m asl. The EC data processing and analysis of the wind, motion, and spectrometer measurements for CO<sub>2</sub> fluxes during SWERUS-C3, using well-established methods for correction of

platform motion (30, 31), have been previously described in detail (32). The initial data processing for CH<sub>4</sub> fluxes was identical to that for CO<sub>2</sub>.

The LGR spectrometer was mounted in a weatherproof box at the base of the mast and connected to the mast inlet with 9.7 m of 10-mm-outer diameter Synflex tubing. Mounted alongside the inlet were a three-dimensional (3D) sonic anemometer (Metek USA-1, METEK GmbH, Elmshorn, Germany) and an XSENS MTi-G-700 (Xsens Technologies B.V., Enschede, The Netherlands) inertial navigation unit providing position, roll, pitch, yaw, and 3D acceleration vectors. EC flux measurements were accepted only when air flow was within 0° ± 120° from the bow based on a computational fluid dynamics model of airflow around *Oden* (33). The model also provided mean wind speed corrections for flow distortion over the ship (34). Additional details of the EC system are provided in (32). For our 20-m asl measurement height, the EC flux footprint extends out to ~1 km, but with large variations due to wind speed, atmospheric surface layer stability, and surface roughness, with a peak contribution from a few hundred meters ahead of the ship. For horizontal wind speed determination, measured winds from the top of the 20-m mast top were adjusted to 10-m height equivalent ( $U_{10}$ ).

A second, identical, and independent cavity ring-down laser spectrometer was also used during SWERUS-C3 for measuring CH<sub>4</sub> and CO<sub>2</sub> concentrations at 1 Hz from four inlets along a 9- to 28-m asl height gradient. A fifth inlet at 4 m asl was also used when the ship was at anchor. Simultaneous continuous measurements of surface water CH<sub>4</sub> from the ship's inlet at 8 m below the surface were made, and the two were used to calculate sea-air CH<sub>4</sub> fluxes based on the bulk flux model of (35). Data obtained along a portion of the cruise track (DoY 192 to 222) were previously presented (4). Here, we follow the same methodology and data processing, albeit with a slightly stricter CO<sub>2</sub> limit (<410 ppm) to avoid possibly ship- and shore-contaminated air when near the Alaskan coast and Barrow. We extended the record with additional atmospheric CH<sub>4</sub> concentration data obtained from the same system until DoY 240, although fewer data were usable in the latter portion of the cruise due to more frequent winds from excluded sectors.

Recent EC CH<sub>4</sub> measurements made from land stations (and therefore not subject to ship motion–induced noise) have been reported to have a limit of quantification of 0.32 mg m<sup>-2</sup> day<sup>-1</sup> or 20 μmol m<sup>-2</sup> day<sup>-1</sup> (36). We evaluated noise in our dataset by examining regions where surface water CH<sub>4</sub> was low and no substantial flux was calculated or observed, and/or that were distant from any seafloor gas seeps (DoY 193 and 211 in heavy ice and DoY 204 and 234 in open water). These days were assumed to represent close to the zero flux level. A histogram of EC fluxes (fig. S1) obtained during these days peaks at +0.25 mg m<sup>-2</sup> day<sup>-1</sup>, a small offset from zero, which may represent the emission in these areas or be due to instrument noise. The 1σ from zero is at ~±1 mg m<sup>-2</sup> day<sup>-1</sup>, and 2σ is ~±2 mg m<sup>-2</sup> day<sup>-1</sup>. We regarded ±1 mg m<sup>-2</sup> day<sup>-1</sup> as the noise for one 20-min sample in our EC CH<sub>4</sub> flux dataset; note that each measurement is independent such that when averaging  $n$  measurements together, the noise decreases by the square root of  $n$ . It is possible to imagine scenarios where a briefly observed flux <1 mg m<sup>-2</sup> day<sup>-1</sup> is predicted by a bulk model but is not quantifiable with EC from a single 20-min measurement.

In total, we reported here 2642 20-min EC CH<sub>4</sub> flux measurements that passed ship motion and wind direction limits (our “temporal” dataset). Because *Oden* spent considerable time anchored or drifting slowly at certain stations during the cruise, with these stations

often selected because of the presence of seafloor gas seeps, the temporal dataset could potentially be biased toward near-seep measurements. Therefore, we spatially normalized the dataset, following the method described in (4). Briefly, GPS latitudes and longitudes were rounded to the nearest  $0.001^\circ$ , and all measurements within that grid cell were combined. A  $0.001^\circ \times 0.001^\circ$  grid cell is approximately  $111 \times 102$  m at  $75^\circ\text{N}$  latitude; for comparison, *Oden* is 108 m in length with a beam of 31 m. Because of the long duration (20 min) of the EC averaging period, the overall difference between the temporally and spatially normalized datasets was small; the spatially normalized dataset contains 2499 total EC flux measurements (compared to 2642 in the temporal dataset). A total of 46 additional measurements were removed because of  $\text{CH}_4$  flux  $< -6 \text{ mg m}^{-2} \text{ day}^{-1}$  and wind speeds  $< 1 \text{ m s}^{-1}$ . The  $\text{CH}_4$  flux lower limit of  $-6 \text{ mg m}^{-2} \text{ day}^{-1}$  (negative fluxes are  $\text{CH}_4$  moving into the seawater) was determined as more than  $5\sigma$  below the average of the mean of background, non-seafloor bubble-influenced, observations. These apparent measurements of large fluxes into the sea could arise because of a variety of stochastic factors (32), but importantly, the observed sea  $\text{CH}_4$  concentrations (4) could not support air-into-seawater fluxes of this scale. Applying these filters and limits did not significantly change the mean observed EC  $\text{CH}_4$  fluxes in any study area, including in the vicinity of seafloor gas seeps.

Because *Oden* was rarely making gridded paths through the sea, the areal extents of the seep areas were somewhat uncertain. However, to be very wrong, the extent of the seep areas would have to exist as long linear formations, which *Oden* coincidentally and consistently crossed perpendicularly. Because *Oden* was actively seeking to visit the seep locations during SWERUS-C3, such a coincidence seems highly unlikely, and we regarded our estimated seep areal extents as generously large, rather than small, estimates.

The extent of "seep areas" of greatly enhanced  $\text{CH}_4$  emissions was determined by defining a minimum and maximum latitude and longitude around EC-determined emission peaks, where emissions remained  $> 6 \text{ mg m}^{-2} \text{ day}^{-1}$ , and calculating the rectangular area within those boundaries. This is necessarily a generous areal estimate. For calculating regional  $\text{CH}_4$  fluxes, we used the spatial limits of seas as determined by continental shelf area and shelf break (7), which places the seaward limit of the shelf seas near the top of the continental slope. The seafloor gas seeps in the Laptev and East Siberian seas were also noted during the cruise by sonar localization of bubbles in the water column, but the sonar data are otherwise unused in our present analysis.

We noted that sea-air bulk flux models could produce incorrect results in ice-covered regions due to the gradient-driven flux being blocked, at least in part, by the ice cover (37). However, recent work has suggested that actual fluxes should scale linearly with open water fraction in areas of partial sea ice coverage (32), although the linear scaling is currently debated in the literature (38). In the ice-covered East Siberian Sea during SWERUS-C3, where the largest calculated  $\text{CH}_4$  fluxes were noted, these bulk fluxes were previously treated as hypothetical because of the ice coverage (4). The use of EC has allowed us to revisit this and avoid the complications of scaling with ice coverage. Our data show that sea-air fluxes in the East Siberian Sea were actually similarly localized as in the ice-free Laptev Sea during SWERUS-C3 (Fig. 2 and Table 2).

Some earlier work [e.g., (24)] has determined ebullition (bubble) fluxes as the difference between a bulk flux and an EC flux; we do not believe that this is a valid approach. A bulk flux estimate was

derived from a local and effectively near-instantaneous measurement of the concentration difference between air and water, scaled by a wind speed-dependent transfer coefficient. A direct EC estimate of the flux is a true measure of the flux (i.e., one with a quantifiable uncertainty) at the measurement location over the specific time interval of the measurement—here, 20 min, sufficient to include all the turbulent eddy scales contributing to the flux. Neither is necessarily representative of the wider regional flux, even on relatively small scales (hundreds of meters), unless certain assumptions are valid. A single EC flux measurement is usually considered to represent the mean interfacial flux over a 2D upwind footprint, the extent of which depends on the measurement height and atmospheric surface layer thermodynamic and turbulent conditions. In our case, for measurements at approximately 20 m asl, typical values would be for 80% of the flux to come from within  $\sim 1$  km upwind, with a peak contribution from  $\sim 100$  m or so upwind (39). The bulk flux estimate was implicitly assumed to represent the same footprint. It was assumed, however, that the forcing conditions—air and water side  $\text{CH}_4$  concentration—are spatially homogeneous across the full extent of the footprint. In the vicinity of a seep, this is unlikely to be the case. For spatially highly heterogeneous conditions, the relative magnitudes of bulk and EC flux estimates will depend on the spatial distribution of the sea-air concentration difference within the flux footprint and in the case of any direct gas transfer from bubbles, the precise location where bubbles break the surface, and potentially the precise set of turbulent eddies sampled for a given measurement.

EC  $\text{CH}_4$  flux results presented here were collected between 11 July (DoY 192) and 28 August (DoY 240) and so encompass not only the Laptev and East Siberian seas discussed previously (4) but also a large section of the Chukchi Sea not previously surveyed with an EC system. The time period for which EC  $\text{CH}_4$  flux data are available extends beyond that of the bulk diffusive flux estimates reported previously (4). The  $\text{CH}_4$  in-water measurement system was not operated after 17 August (DoY 229). The EC system, however, operated autonomously and collected  $\text{CH}_4$  flux data in ice-free regions of the Chukchi Sea and eastern East Siberian Sea until DoY 240 (28 August). Mirror degradation in the spectrometer used for EC measurements, caused by sea salt buildup, prevented flux measurements after this date.

We noted that a bulk diffusive flux model has no lower limit to fluxes; fluxes simply approach zero as the wind speed drops, although a commonly used model is calibrated for winds in the range of 3 to  $15 \text{ m s}^{-1}$  (35). An EC system, in contrast, can measure fluxes at lower horizontal wind speeds than are recommended for the bulk flux models. As noted above, these EC measured fluxes could be due to processes such as gas bubbles reaching the water surface and bursting. However, in the present study, ship emissions and flow distortion considerations limit our ability to incorporate data where wind speed is  $< 1 \text{ m s}^{-1}$ . In addition, because the waterside  $\text{CH}_4$  concentration measurements used in (4) were from 8-m depth, it is possible that concentrations nearer the surface differ and therefore that waterside measurements when wind-driven diffusive fluxes are significant would tend to yield calculated diffusive fluxes larger than actual fluxes measured by EC. However, CTD (conductivity-temperature-depth) dissolved gas profiles suggest that the surface mixed layer extended below 8-m depth throughout the cruise (32).

Sea ice coverage was determined visually and by satellite retrieval provided by the University of Bremen using the Advanced Microwave Scanning Radiometer 2 (AMSR2) at 89 MHz on the Japanese "Shizuku" [GCOM-W (Global Change Observation Mission-Water)] satellite

(40). The retrieved coverage is similar to that from the SSMIS (Special Sensor Microwave Imager/Sounder) instruments, as used in (4).

## SUPPLEMENTARY MATERIALS

Supplementary material for this article is available at <http://advances.sciencemag.org/cgi/content/full/6/5/eaay7934/DC1>

Fig. S1. Histogram of EC CH<sub>4</sub> sea-air 20-min flux measurements away from gas seeps.

Fig. S2. HYSPLIT back trajectory for Chukchi Sea enhanced CH<sub>4</sub> (21 August 2014).

Fig. S3. HYSPLIT back trajectory for Chukchi Sea enhanced CH<sub>4</sub> (27 August 2014).

## REFERENCES AND NOTES

- E. A. G. Schuur, A. D. McGuire, C. Schadel, G. Grosse, J. W. Harden, D. J. Hayes, G. Hugelius, C. D. Koven, P. Kuhry, D. M. Lawrence, S. M. Natali, D. Olefeldt, V. E. Romanovsky, K. Schaefer, M. R. Turetsky, C. C. Treat, J. E. Vonk, Climate change and the permafrost carbon feedback. *Nature* **520**, 171–179 (2015).
- N. Shakhova, I. Semiletov, I. Leifer, V. Sergienko, A. Salyuk, D. Kosmach, D. Chernykh, C. Stubbs, D. Nicolov, V. Tumskoy, Ö. Gustafsson, Ebullition and storm-induced methane release from the East Siberian Arctic Shelf. *Nat. Geosci.* **7**, 64–70 (2014).
- A. Berchet, P. Bousquet, I. Pison, R. Locatelli, F. Chevallier, J. D. Paris, E. J. Dlugokencky, T. Laurila, J. Hatakka, Y. Viisanen, D. E. J. Worthy, E. Nisbet, R. Fisher, J. France, D. Lowry, V. Ivakhov, O. Hermansen, Atmospheric constraints on the methane emissions from the East Siberian Shelf. *Atmos. Chem. Phys.* **16**, 4147–4157 (2016).
- B. F. Thornton, M. C. Geibel, P. M. Crill, C. M. Mörtz, Methane fluxes from the sea to the atmosphere across the Siberian shelf seas. *Geophys. Res. Lett.* **43**, 5869–5877 (2016).
- J. W. Pohlman, J. Greinert, C. Ruppel, A. Silyakova, L. Vielstädte, M. Casso, J. Mienert, S. Bünz, Enhanced CO<sub>2</sub> uptake at a shallow Arctic Ocean seep field overwhelms the positive warming potential of emitted methane. *Proc. Natl. Acad. Sci. U.S.A.* **114**, 5355–5360 (2017).
- E. A. Kort, S. C. Wofsy, B. C. Daube, M. Diao, J. W. Elkins, R. S. Gao, E. J. Hints, D. F. Hurst, R. Jimenez, F. L. Moore, J. R. Spackman, M. A. Zondlo, Atmospheric observations of Arctic Ocean methane emissions up to 82° north. *Nat. Geosci.* **5**, 318–321 (2012).
- M. Jakobsson, Hypsometry and volume of the Arctic Ocean and its constituent seas. *Geochem. Geophys. Geosyst.* **3**, 1–18 (2002).
- C. Stranne, M. O'Regan, M. Jakobsson, Overestimating climate warming-induced methane gas escape from the seafloor by neglecting multiphase flow dynamics. *Geophys. Res. Lett.* **43**, 8703–8712 (2016).
- D. S. Baer, J. Greinert, Y. Artemov, S. E. Beaubien, A. Wuest, Fate of rising methane bubbles in stratified waters: How much methane reaches the atmosphere? *J. Geophys. Res.* **111**, (2006).
- B. B. Ward, K. A. Kilpatrick, A. E. Wopat, E. C. Minnich, M. E. Lidstrom, Methane oxidation in Saanich inlet during summer stratification. *Cont. Shelf Res.* **9**, 65–75 (1989).
- K. J. Sparrow, J. D. Kessler, J. R. Southon, F. Garcia-Tigueros, K. M. Schreiner, C. D. Ruppel, J. B. Miller, S. J. Lehman, X. Xu, Limited contribution of ancient methane to surface waters of the U.S. Beaufort Sea shelf. *Sci. Adv.* **4**, eaao4842 (2018).
- C. L. Myhre, B. Ferré, S. M. Platt, A. Silyakova, O. Hermansen, G. Allen, I. Pisso, N. Schmidbauer, A. Stohl, J. Pitt, P. Jansson, J. Greinert, C. Percival, A. M. Fjaeraa, S. J. O'Shea, M. Gallagher, M. Le Breton, K. N. Bower, S. J. B. Bauguitte, S. Dalsøren, S. Vadakkepuliambatta, R. E. Fisher, E. G. Nisbet, D. Lowry, G. Myhre, J. A. Pyle, M. Cain, J. Mienert, Extensive release of methane from Arctic seabed west of Svalbard during summer 2014 does not influence the atmosphere. *Geophys. Res. Lett.* **43**, 4624–4631 (2016).
- W. S. Reeburgh, Anaerobic methane oxidation: Rate depth distributions in Skan Bay sediments. *Earth Planet. Sci. Lett.* **47**, 345–352 (1980).
- P. P. Overduin, S. Liebner, C. Knoblauch, F. Günther, S. Wetterich, L. Schirmermeister, H.-W. Hubberten, M. N. Grigoriev, Methane oxidation following submarine permafrost degradation: Measurements from a central Laptev Sea shelf borehole. *J. Geophys. Res. Biogeosci.* **120**, 965–978 (2015).
- B. F. Thornton, M. Wik, P. M. Crill, Double-counting challenges the accuracy of high-latitude methane inventories. *Geophys. Res. Lett.* **43**, 12569–12577 (2016).
- M. Saunio, P. Bousquet, B. Poulter, A. Peregón, P. Ciais, J. G. Canadell, E. J. Dlugokencky, G. Etiope, D. Bastviken, S. Houweling, G. Janssens-Maenhout, F. N. Tubiello, S. Castaldi, R. B. Jackson, M. Alexe, V. K. Arora, D. J. Beerling, P. Bergamaschi, D. R. Blake, G. Brailsford, V. Brovkin, L. Bruhwiler, C. Creveling, P. Crill, K. Covey, C. Curry, C. Frankenberg, N. Gedney, L. Höglund-Isaksson, M. Ishizawa, A. Ito, F. Joos, H. S. Kim, T. Kleinen, P. Krummel, J. F. Lamarque, R. Langenfelds, R. Locatelli, T. Machida, S. Maksyutov, K. C. McDonald, J. Marshall, J. R. Melton, I. Morino, V. Naik, S. O'Doherty, F. J. W. Parmentier, P. K. Patra, C. Peng, S. Peng, G. P. Peters, I. Pison, C. Prigent, R. Prinn, M. Ramonet, W. J. Riley, M. Saito, M. Santini, R. Schroeder, I. J. Simpson, R. Spahn, P. Steele, A. Takizawa, B. F. Thornton, H. Tian, Y. Tohjima, N. Viovy, A. Voulgarakis, M. van Weele, G. R. van der Werf, R. Weiss, C. Wiedinmyer, D. J. Wilton, A. Wiltshire, D. Worthy, D. Wunch, X. Xu, Y. Yoshida, B. Zhang, Z. Zhang, Q. Zhu, The global methane budget 2000–2012. *Earth Syst. Sci. Data* **8**, 697–751 (2016).
- K. A. Kvenvolden, M. D. Lilley, T. D. Lorenson, P. W. Barnes, E. McLaughlin, The Beaufort Sea continental shelf as a seasonal source of atmospheric methane. *Geophys. Res. Lett.* **20**, 2459–2462 (1993).
- C. Stranne, M. O'Regan, G. R. Dickens, P. Crill, C. Miller, P. Preto, M. Jakobsson, Dynamic simulations of potential methane release from East Siberian continental slope sediments. *Geochem. Geophys. Geosyst.* **17**, 872–886 (2016).
- K. B. Bartlett, R. C. Harriss, Review and assessment of methane emissions from wetlands. *Chemosphere* **26**, 261–320 (1993).
- M. Tjernström, M. D. Shupe, I. M. Brooks, P. O. G. Persson, J. Prytherch, D. J. Salisbury, J. Sedlar, P. Achtert, B. J. Brooks, P. E. Johnston, G. Sotiropoulou, D. Wolfe, Warm-air advection, air mass transformation and fog causes rapid ice melt. *Geophys. Res. Lett.* **42**, 5594–5602 (2015).
- A. S. Savvichev, I. I. Rusanov, N. V. Pimenov, E. E. Zakharova, E. F. Veslopolova, A. Y. Lein, K. Crane, M. V. Ivanov, Microbial processes of the carbon and sulfur cycles in the Chukchi Sea. *Microbiology* **76**, 603–613 (2007).
- D. A. Kosmach, V. I. Sergienko, O. V. Dudarev, A. V. Kurilenko, O. Gustafsson, I. P. Semiletov, N. E. Shakhova, Methane in the surface waters of Northern Eurasian marginal seas. *Dokl. Chem.* **465**, 281–285 (2015).
- L. Fenwick, D. Capelle, E. Damm, S. Zimmermann, W. J. Williams, S. Vagle, P. D. Tortell, Methane and nitrous oxide distributions across the North American Arctic Ocean during summer, 2015. *J. Geophys. Res. Oceans* **122**, 390–412 (2017).
- N. Shakhova, I. Semiletov, A. Salyuk, V. Yusupov, D. Kosmach, Ö. Gustafsson, Extensive methane venting to the atmosphere from sediments of the East Siberian Arctic Shelf. *Science* **327**, 1246–1250 (2010).
- N. Kijun, P. Calanca, M. W. Rotach, H. P. Schmid, A simple two-dimensional parameterisation for Flux Footprint Prediction (FFP). *Geosci. Model Dev.* **8**, 3695–3713 (2015).
- A. F. Stein, R. R. Draxler, G. D. Rolph, B. J. B. Stunder, M. D. Cohen, F. Ngan, NOAA's HYSPLIT atmospheric transport and dispersion modeling system. *Bull. Am. Meteorol. Soc.* **96**, 2059–2077 (2015).
- K. R. Barnhart, C. R. Miller, I. Overeem, J. E. Kay, Mapping the future expansion of Arctic open water. *Nat. Clim. Chang.* **6**, 280–285 (2016).
- W. R. McGillis, J. B. Edson, J. E. Hare, C. W. Fairall, Direct covariance air-sea CO<sub>2</sub> fluxes. *J. Geophys. Res. Oceans* **106**, 16729–16745 (2001).
- M. Yang, J. Prytherch, E. Kozlova, M. J. Yelland, D. Parenkat Mony, T. G. Bell, Comparison of two closed-path cavity-based spectrometers for measuring air–water CO<sub>2</sub> and CH<sub>4</sub> fluxes by eddy covariance. *Atmos. Meas. Tech.* **9**, 5509–5522 (2016).
- D. S. Baer, J. B. Paul, M. Gupta, A. O'Keefe, Sensitive absorption measurements in the near-infrared region using off-axis integrated-cavity-output spectroscopy. *Appl. Phys. B* **75**, 261–265 (2002).
- J. B. Edson, A. A. Hinton, K. E. Prada, J. E. Hare, C. W. Fairall, Direct covariance flux estimates from mobile platforms at sea. *J. Atmos. Ocean. Technol.* **15**, 547–562 (1998).
- J. Prytherch, M. J. Yelland, I. M. Brooks, D. J. Tupman, R. W. Pascal, B. I. Moat, S. J. Norris, Motion-correlated flow distortion and wave-induced biases in air–sea flux measurements from ships. *Atmos. Chem. Phys.* **15**, 10619–10629 (2015).
- J. Prytherch, I. M. Brooks, P. M. Crill, B. F. Thornton, D. J. Salisbury, M. Tjernström, L. G. Anderson, M. C. Geibel, C. Humborg, Direct determination of the air-sea CO<sub>2</sub> gas transfer velocity in Arctic sea ice regions. *Geophys. Res. Lett.* **44**, 3770–3778 (2017).
- B. I. Moat, M. J. Yelland, I. M. Brooks, in *NOC Internal Report 17* (National Oceanography Centre, 2015).
- M. J. Yelland, B. I. Moat, R. W. Pascal, D. I. Berry, CFD model estimates of the airflow distortion over research ships and the impact on momentum flux measurements. *J. Atmos. Ocean. Technol.* **19**, 1477–1499 (2002).
- R. Wanninkhof, Relationship between wind speed and gas exchange over the ocean revisited. *Limnol. Oceanogr. Methods* **12**, 351–362 (2014).
- M. Yang, T. G. Bell, F. E. Hopkins, V. Kitidis, P. W. Cazenave, P. D. Nightingale, M. J. Yelland, R. W. Pascal, J. Prytherch, I. M. Brooks, T. J. Smyth, Air–sea fluxes of CO<sub>2</sub> and CH<sub>4</sub> from the Penlee Point Atmospheric Observatory on the south-west coast of the UK. *Atmos. Chem. Phys.* **16**, 5745–5761 (2016).
- B. Loose, L. A. Miller, S. Elliott, T. Papakyriakou, Sea ice biogeochemistry and material transport across the frozen interface. *Oceanography* **24**, 202–218 (2011).
- A. Bigdeli, T. Hara, B. Loose, A. T. Nguyen, Wave attenuation and gas exchange velocity in marginal sea ice zone. *J. Geophys. Res. Oceans* **123**, 2293–2304 (2018).
- G. Spreen, L. Kaleschke, G. Heygster, Sea ice remote sensing using AMSR-E 89-GHz channels. *J. Geophys. Res. Oceans* **113**, C02S03 (2008).

**Acknowledgments:** We thank the two crews of *I/B Oden* who made the SWERUS-C3 expedition possible and those whose efforts in organizing the cruise were vital. Maps were produced using Ocean Data View 4 by R. Schlitzer (<http://odv.awi.de>). **Funding:** SWERUS-C3 funding was provided by the Knut and Alice Wallenberg Foundation, Vetenskapsrådet (Swedish Research Council), the Stockholm University, Polarforskningssekretariatet (Swedish Polar Research Secretariat), the Bolin Centre for Climate Research, and the UK Natural Environment Research Council (grant NE/K011820/1). Additional grants from Vetenskapsrådet to P.C. covering this work: 2014-6584 and 2013-5562. **Author contributions:** B.F.T., J.P., I.M.B., D.S., M.T., and P.M.C. developed, installed, and operated the integrated shipboard system for CH<sub>4</sub> fluxes during SWERUS-C3. B.F.T., J.P., and K.A. processed and analyzed the data. B.F.T. wrote the first version of the manuscript. All authors contributed to the revisions of the manuscript. **Competing interests:** The authors declare that they have no competing interests. **Data and materials**

**availability:** All data needed to evaluate the conclusions in the paper are present in the paper and/or the Supplementary Materials and/or the raw data, archived at the Bolin Centre for Climate Research database: <https://bolin.su.se/data>.

Submitted 18 July 2019

Accepted 22 November 2019

Published 29 January 2020

10.1126/sciadv.aay7934

**Citation:** B. F. Thornton, J. Prytherch, K. Andersson, I. M. Brooks, D. Salisbury, M. Tjernström, P. M. Crill, Shipborne eddy covariance observations of methane fluxes constrain Arctic sea emissions. *Sci. Adv.* **6**, eaay7934 (2020).

## Shipborne eddy covariance observations of methane fluxes constrain Arctic sea emissions

Brett F. Thornton, John Prytherch, Kristian Andersson, Ian M. Brooks, Dominic Salisbury, Michael Tjernström and Patrick M. Crill

*Sci Adv* 6 (5), eaay7934.  
DOI: 10.1126/sciadv.aay7934

ARTICLE TOOLS	<a href="http://advances.sciencemag.org/content/6/5/eaay7934">http://advances.sciencemag.org/content/6/5/eaay7934</a>
SUPPLEMENTARY MATERIALS	<a href="http://advances.sciencemag.org/content/suppl/2020/01/27/6.5.eaay7934.DC1">http://advances.sciencemag.org/content/suppl/2020/01/27/6.5.eaay7934.DC1</a>
REFERENCES	This article cites 38 articles, 3 of which you can access for free <a href="http://advances.sciencemag.org/content/6/5/eaay7934#BIBL">http://advances.sciencemag.org/content/6/5/eaay7934#BIBL</a>
PERMISSIONS	<a href="http://www.sciencemag.org/help/reprints-and-permissions">http://www.sciencemag.org/help/reprints-and-permissions</a>

Use of this article is subject to the [Terms of Service](#)

---

*Science Advances* (ISSN 2375-2548) is published by the American Association for the Advancement of Science, 1200 New York Avenue NW, Washington, DC 20005. The title *Science Advances* is a registered trademark of AAAS.

Copyright © 2020 The Authors, some rights reserved; exclusive licensee American Association for the Advancement of Science. No claim to original U.S. Government Works. Distributed under a Creative Commons Attribution NonCommercial License 4.0 (CC BY-NC).